

# RESEARCH MEMORANDUM

INVESTIGATION OF ENGINE PERFORMANCE AND HIGH-TEMPERATURE  
PROPERTIES OF PRECISION-CAST TURBINE BLADES  
OF HIGH-CARBON STELLITE 21 AND  
CONTROLLED-GRAIN-SIZE STELLITE 21

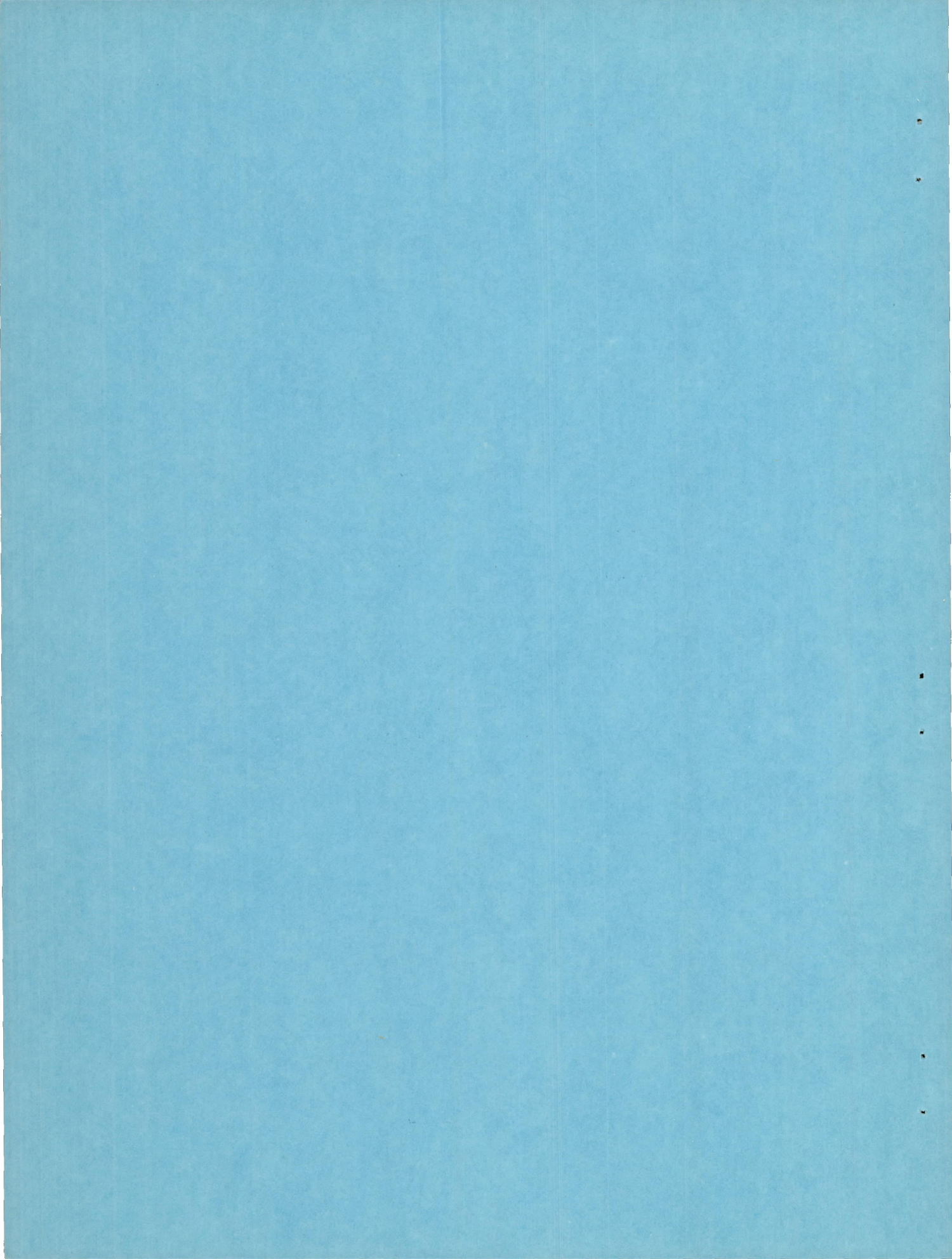
By Charles Yaker, Floyd B. Garrett, and Paul F. Sikora

Lewis Flight Propulsion Laboratory  
Cleveland, Ohio

CASE FILE  
COPY

NATIONAL ADVISORY COMMITTEE  
FOR AERONAUTICS

WASHINGTON  
June 23, 1952



## NATIONAL ADVISORY COMMITTEE FOR AERONAUTICS

RESEARCH MEMORANDUMINVESTIGATION OF ENGINE PERFORMANCE AND HIGH-TEMPERATURE  
PROPERTIES OF PRECISION-CAST TURBINE BLADES OF HIGH-CARBON  
STELLITE 21 AND CONTROLLED-GRAIN-SIZE STELLITE 21

By Charles Yaker, Floyd B. Garrett, and Paul F. Sikora

## SUMMARY

An investigation was conducted to determine the effect of controlled grain size and increased carbon content on engine performance and high-temperature properties of precision-cast Stellite 21 turbine blades. Blades were cast to result in controlled grain sizes, classed as fine, medium, and coarse. Other blades were cast of high-carbon Stellite 21. The blades were mounted in a Timken 16-25-6 rotor and operated in a U. S. Air Force J33-9 turbojet engine in 20-minute cycles consisting of 15 minutes at rated speed and approximately 5 minutes at idle speed. Laboratory stress-rupture tests of specimens cut from blades were conducted at the stress and temperature conditions encountered during rated-speed operation in the engine.

The results of the engine test and the laboratory stress-rupture tests indicated:

1. Fine-grain Stellite 21 blades had a lower life and creep resistance than the medium- and coarse-grain blades, and all three grain size blades manifested less scatter than the production blades.
2. High-carbon Stellite 21 had higher blade life than the production Stellite 21.

## INTRODUCTION

The turbojet engine component operating under the most severe combination of stress and temperature is the turbine blade. In order to meet the stress and temperature requirements for the turbine blades, a number of heat-resistant alloys have been developed. The majority of these alloys are fabricated into turbine blades by one of two methods: forging or precision casting. Blades made by either method have found

wide application in the jet engine fields. In order to meet present and future demands for turbine blades, both the forging and the precision casting facilities must be utilized. For several years there has been a definite trend away from the use of precision-cast blades in turbojet engines because of the wide scatter of blade performance of the precision-cast alloys, which resulted in unpredictable early failures in turbojet engines.

The Lewis laboratory of the NACA has been conducting an investigation of the mechanisms of failure in turbine blades made from cast alloys and the effects of fabrication variables on the blade performance of these alloys. As part of this program, precision-cast blades of production Stellite 21, high-carbon Stellite 21, and fine-, medium-, and coarse-grain Stellite 21 produced by control of casting temperatures were mounted in a Timken 16-25-6 rotor and operated in a U.S. Air Force J33-9 turbojet engine. The test consisted of a repetition of a 20-minute cycle (15 min at rated speed and approximately 5 min at idle). Cyclic operation was employed to simulate actual service conditions. The engine was shut down at the close of the work day or whenever a turbine blade failed. At shut-down intervals during the engine operation, the turbine blades were measured to determine the amount of blade creep and were inspected for damage. The blades were operated to failure. At the conclusion of operation, all blade failures were examined metallogically to determine the nature of the failure and the structural changes occurring in the blades during operation.

In order to compare the results of the engine tests with laboratory data, the high-temperature strength of the materials was determined. This determination was made by stress-rupture testing of specimens cut from blades. The tests were conducted at the stress and temperature conditions encountered during rated-speed operation of the engine.

#### APPARATUS AND PROCEDURE

Turbine blades. - The blade alloys investigated and their chemical compositions are listed in table I. These alloys were precision cast into turbine blades and given the following heat treatments:

Type of Stellite 21	Number of blades in wheel	Heat treatment
Production	6	None
High carbon	6	None
Fine grain	4	24 hours at 1350° F
Medium grain	9	24 hours at 1350° F
Coarse grain	5	24 hours at 1350° F

The controlled-grain-size blades were produced by a variation of pouring temperature at a fixed mold temperature. Fabrication details are given in reference 1. All blades were radiographed for flaws.

The Timken alloy rotor was fitted with 52 standard blades and two blades fitted with thermocouples as described in reference 2. (Part of the blades in the wheel were for another investigation.) Before engine operation, the cross-sectional areas of several blades of each type were measured on an optical comparator, and the stress distributions along the airfoil were calculated by the method described in reference 3.

Engine operation. - The blades were operated in a U. S. Air Force J33-9 turbojet engine having a nominal thrust of 4000 pounds and employing a dual-entry centrifugal compressor. The engine has 14 combustion chambers. The engine and test instrumentation are described in reference 4. The engine test consisted of a repetition of the cycle shown in figure 1. During the rated-speed portion of the cycle, the gas temperature was varied to yield a temperature of  $1475 \pm 5^{\circ}$  F measured 2 inches from the base of the thermocoupled half blade. This procedure would result in a temperature of  $1500 \pm 5^{\circ}$  F at the midpoint of a full blade (reference 2).

Three blades of each alloy sample were scribed in the manner shown in figure 2. At shut-down periods during engine operation, measurements were made of blade creep between these scribed marks with an optical extensometer having a reading accuracy of  $\pm 0.0001$  inch. After a failure, the blades were examined for damage resulting from failure of blades or of other engine components and the location and nature of the damage were recorded. All blades were operated to failure, defined as either complete blade fracture or evidence of the beginning of fracture. In order to minimize the damage resulting from blade fracture, the thickness of the shroud in the engine tail cone surrounding the turbine wheel was reduced to allow blade fragments to pierce the tail cone easily and to be thrown clear of the turbine.

Metallurgical examination of blades. - As-received and tested blades were examined to determine any metallurgical changes that occurred during engine operation and the mechanism of the failure propagation. The examinations were made with standard metallurgical equipment and procedures.

High-temperature strength evaluations. - Simultaneously with the engine operations, stress-rupture tests were conducted on specimens cut from the airfoil sections of blades from the same lots as those used in the engine test. The shape of the specimen and the zone of the blade from which it was machined are shown in figure 3. The zone of the blade from which the specimen was cut was selected to give a maximum amount of stock for a specimen having the gage section in the mid-zone (also the failure zone of the airfoil section). The stress-

rupture tests were all conducted at 1500° F in machines by means of a loading system which consisted of a simple beam acting through a system of knife edges. The specimens were heated in a resistance-type furnace. The specimen temperature was controlled until there was less than a 5° F variation along the length of the specimen, with the average temperature varying only  $\pm 3^\circ$  F.

## RESULTS

### Blade Stresses

From the results of the determinations of the centrifugal stress distributions at rated speed (11,500 rpm) of test blades, the stress was determined for each blade sample 2 inches above the base of the blade (the point of maximum temperature (reference 5)). The average values of this stress for each alloy are listed in table II.

### Engine Operation

The wheel containing the test blades was operated for a total of 508 cycles or approximately 127 hours at rated speed. The test was concluded at this time because of severe damage to the blades caused by the failure of another engine component. The complete results of engine operation are listed in table III. Failure time is considered as the time at rated speed (11,500 rpm) only. Because the temperature and stress conditions during the idle portion of the cycle are low, this time is neglected in determining the life of the blades. In further evaluations of the results of the engine test, the failures resulting from impact damage will be omitted because they are the result of extraordinary operating conditions and are therefore not indicative of the true performance of an alloy.

The results of the blade-creep measurements indicate that the zone of maximum creep lay just above or below the middle of the blade airfoil section. In general, the section of maximum elongation was either section 3 or 4, the sections just below or above the middle of the blades. In figure 4, the creep curves for sections 3 and 4 are plotted for all the scribed test blades. The final blade elongations in zones 3 and 4 prior to failure for true blade failures (not resulting from damage) are listed in table IV. For purposes of comparison, the values of creep over zones 3 and 4 were averaged for the scribed blades in each group and a qualitative comparison of the blade creep is shown in figure 5.

### Metallurgical Examination

The results of the metallurgical examination are presented in figures 6 to 8, which present the nature of the blade failures and the changes in blade structure during operation. The microstructures shown were selected to represent the various groups of blades.

The results of the metallurgical examinations of the blade failures indicate that the failures were of the following types:

(1) In figure 9(a) are shown failures in which the origin of the fracture is characterized by an irregular granular surface showing no evidence of fatigue-type failure. The fracture follows an intercrystalline path and small intercrystalline cracks are present in the area just below the failure zone. Because of the similarity of such failures to those encountered in laboratory stress-rupture tests, these failures were classed as the stress-rupture type.

(2) The failures of figure 9(b) are characterized by a smooth fracture surface at the failure origin, sometimes showing the familiar concentric ring markings of a fatigue failure. These failures follow a transcrystalline path. In this class fall the failures that result from the combined effects of the centrifugal and vibratory stresses and show no evidence of initiation of the stress-rupture type of failure. These failures were classed as the fatigue type.

(3) In the failures of figure 9(c), the fracture originated in a zone similar to that described for the stress-rupture-type failure, and then progressed through a zone of the fatigue-type failure. The stress-rupture origin of these failures is determined by macroscopic and microscopic examination of both the initial cracks detected during operation and the final fracture. These failures will be classed as the stress-rupture-followed-by-fatigue type.

The preceding classification of failures refers only to the beginning zones of blade failure. After fracture has progressed to a critical depth by any of the mentioned types of failure, the blades fail in tension because of the high stresses produced by the reduced load-carrying area. In figure 10, the results of the engine operation are presented and the type of failure mechanism associated with each true blade failure is shown.

The results of the grain-size measurements of the blades are listed in table V. Figure 11 presents a qualitative comparison of the three different grain sizes in the controlled-grain-size blades.

The results of the change in hardness during operation are summarized in table VI. The hardness before operation was determined on the remaining pieces of the blades from which the stress-rupture specimens were machined. The data in table VI indicate that the high-carbon Stellite 21 is slightly harder than the production alloy in the as-cast condition but increased approximately the same amount in hardness during operation. The controlled-grain-size blades in the preoperation condition are all harder than the production Stellite 21 blades by approximately the same amount. The increased hardness is due to the preoperation aging treatment given to the blades. During operation, the controlled-grain-size blades and the production Stellite 21 blades all increased in hardness to an approximately equal value.

The results of the stress-rupture tests from blade specimens are presented in figure 12; also plotted are the blade failures as well as available data on cast rupture-bar specimens of the various alloys.

#### DISCUSSION OF RESULTS

Effect of grain size. - Before the effect of grain size on blade performance is discussed, the probable effect of the casting conditions on structure should be noted. Because the conditions subject the blades to a specific range of temperatures through which the blades cool at a specific rate, each set of casting conditions of the various grain-size groups can be considered as an individual heat treatment. Stellite 21 is structurally sensitive to both temperature and cooling rate (references 6 and 7). Although the various blades are specified by grain size, it should be remembered that the heat treatment to secure the grain size of the blade was a contributing factor in the results obtained.

The results of the engine operation of the controlled-grain-size Stellite 21 blades (fig. 10) indicate that the failure bands are narrower than the bands for the production blades. This fact indicates that the improvement in uniformity of performance is not necessarily a function of grain size but possibly a function of controlling either the casting conditions or the uniformity of the grain size. The number of blades tested in this investigation was too small to make a quantitative comparison of the effects of controlled-grain-size casting on the amount of scatter in the failure band for Stellite 21.

The results of the engine operation of controlled-grain-size Stellite 21 (table III and fig. 10) indicate that fine-grain blades have shorter lives than coarse- and medium-grain blades. The results also indicate that the coarse-grain blades are slightly weaker than the medium-grain blades. However, since the average lives of coarse and medium blades are nearly the same (fig. 10) the difference in strength is probably not significant. The data in reference 1 for cast specimens

tested in stress rupture at the engine stress and temperature conditions confirm the results of the engine tests. The fine-grain specimens gave significantly lower lives than coarse and medium specimens, which had nearly equal stress-rupture lives.

Because all the controlled-grain-size Stellite 21 blades failed primarily by stress-rupture mechanisms, the results of the engine test should agree with the laboratory stress-rupture tests. Comparison of engine results with the laboratory stress-rupture tests on specimens cut from blades (fig. 12) showed that the blade-specimen stress-rupture lives were shorter than the lives obtained in the engine for the blades for all three grain sizes. This result is probably due to the effect of the size of the specimen used for stress-rupture testing. The results in figure 12 show a closer agreement between blade-specimen stress-rupture life and the blade operating life for the fine-grain size than for the coarse-grain size. That is, as the number of grains per cross-section increases (fine grain), the degree of correlation between the blade and blade specimen increases. For blades of large grain size (that is, cast blades), it is apparent that an attempted correlation of blade-material rupture properties and blade life in the engine by this method will not be entirely satisfactory.

The results of the creep measurements of the Stellite 21 controlled-grain-size blades (table IV, figs. 4(a) to 4(c), and fig. 5) indicate that the fine-grain blades have lower creep resistance than the coarse and medium blades. The coarse- and medium-grain blades showed little difference in creep resistance.

One reason for the lack of significant differences in blade life and creep resistance for the coarse- and medium-grain blades is probably the small difference in the grain sizes of the two groups. Both groups have macroscopic grain sizes, 10 to 18 grains per blade cross section for the coarse, and 27 to 51 grains per blade cross section for the medium. The fine-grain blades, however, were appreciably different in grain size from the medium and coarse; the average microscopic size of the fine-grain blades was from A.S.T.M. 2 to 4, or about 3000 to 12,000 grains per blade cross section. The results of the metallurgical examination of the controlled-grain-size Stellite 21 blades also indicate that the blade hardnesses of all grain sizes are very nearly the same before and after operation (table VI). The microstructures of the blades also are similar in the nature of the phases visible. Because the controlled-grain-size blades were similar in structure and hardness, it may then be assumed that the effect of the structure and hardness on the life of the blades would cancel out and leave only the grain size as the controlling factor on blade life.

Effect of increasing carbon content of Stellite 21. - The high-carbon Stellite 21 contains 0.38 percent carbon as compared with 0.28 percent in normal Stellite 21. The 0.10-percent change in carbon content is the only significant difference in the composition of the two alloys. The results of engine operation of the high-carbon blades indicate a significant improvement in blade life over the production Stellite 21 (table III and fig. 10). The production-alloy blades had a life band from about 42 to 82 hours, and the high-carbon alloy, from about 68 to 127 or more hours. The mechanism of blade failure was the same for both alloys, stress rupture followed by fatigue.

A comparison of the creep curves for the high-carbon and the production alloy (figs. 4(d), 4(e), and 5) indicates that within the normal range of scatter there is little difference in creep resistance between the two alloys.

The results of the metallurgical examination of the production and high-carbon alloy indicate some difference in preoperation (as-cast) hardness (table VI). The high-carbon blades were, on the average, 1.3 units on the Rockwell A scale harder than the production blades. Both alloys increased in hardness during operation by the same amount, around 7 units on the Rockwell A scale (table VI).

There was little difference in the preoperation structure of both alloys (fig. 7(d) and 7(f)), although the high-carbon Stellite 21 does show more precipitate at the grain boundaries. After operation, both alloys show an increase in the amount of grain-boundary precipitation (figs. 7(e) and 7(g)); this increase is greater for the high-carbon Stellite 21. Because the precipitates are carbides (reference 8), these changes are as expected. The increased operating life of the high-carbon Stellite 21 blades over the production Stellite 21 may be due to the greater amount of lamellar precipitate of the high-carbon alloy. Investigation of heat-treated supercharger blades of Stellite 21 (reference 7) has indicated that the highest blade life for this alloy may be associated with a lamellar or plate-like precipitate.

#### SUMMARY OF RESULTS

Investigation of the engine performance and laboratory stress-rupture properties of precision-cast turbine blades of the heat-resistant materials, production, high-carbon, and normal Stellite 21 in three different grain sizes, indicated:

1. All three grain sizes (produced by control of casting temperature) had less scatter in blade life than the production Stellite 21. Controlled-grain-size blade specimens of Stellite 21 had less scatter than

the production Stellite 21 or the high-carbon Stellite 21 on the basis of the laboratory stress-rupture tests. Fine-grain blades of Stellite 21 had lower life than the coarse- and medium-grain Stellite 21 blades, which had essentially the same blade life.

2. Fine-grain blades of Stellite 21 had lower creep resistance during engine operation than the coarse- and medium-grain blades, which had essentially the same creep resistance.

3. High-carbon Stellite 21 with an increased carbon content of 0.10 percent over production Stellite 21 had a significantly higher engine blade life than the production alloy. The increased carbon content did not change the creep resistance of the Stellite 21 blades.

Lewis Flight Propulsion Laboratory  
National Advisory Committee for Aeronautics  
Cleveland, Ohio

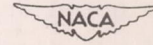
#### REFERENCES

1. Hamilton, N. E., and Grant, N. J.: Controlled Grain Size, Precision Cast Turbine Blades. (BuShips, Navy Dept. Contract NObs-25391. Tasks No. 10 - 12.)
2. Garrett, F. B., and Yaker, C.: Relation of Engine Turbine-Blade Life to Stress-Rupture Properties of the Alloys, Stellite 21, Hastelloy B, Cast S-816, Forged S-816, X-40, Nimonic 80, Refractalloy 26, N-155, and Inconel X. NACA RM E51G13, 1951.
3. Kemp, Richard H., and Morgan William C.: Analytical Investigation of Distribution of Centrifugal Stresses and Their Relation to Limiting Operating Temperatures in Gas-Turbine Blades. NACA RM E7L05, 1948.
4. Farmer, J. Elmo, Darmara, F. N., and Poulson, Francis D.: Cyclic Engine Test of Cast Vitallium Turbine Buckets - I. NACA RM E7J23, 1948.
5. Farmer, J. Elmo: Relation of Nozzle-Blade and Turbine-Bucket Temperatures to Gas Temperatures in a Turbojet Engine. NACA RM E7L12, 1948.
6. Yaker, C., and Hoffman, C. A.: Effects of Some Solution Treatments Followed by an Aging Treatment on the Life of Small Cast Gas-Turbine Blades of a Cobalt-Chromium-Base Alloy. I - Effect of Solution-Treating Temperature. NACA TN 2320, 1951.

7. Hoffman, C. A., and Robards, C. F.: Effects of Some Solution Treatments Followed by an Aging Treatment on the Life of Small Cast Gas-Turbine Blades of a Cobalt-Chromium-Base Alloy. II - Effect of Selected Combinations of Soaking Time, Temperature, and Cooling Rate. NACA TN 2513, 1951.
8. Lane, J. R., and Grant, N. J.: Carbide Reactions in High Temperature Alloys. Preprint No. 10, Am. Soc. Metals Trans., 1951, vol. 44, 1952.
9. Anon.: Haynes Alloys for High-Temperature Service. Haynes Stellite Co. (Kokomo, Ind.), 1948.

TABLE I - NOMINAL CHEMICAL COMPOSITION OF PRECISION-CAST ALLOYS

EVALUATED AS TURBINE BLADES



Alloy	C	Co	Cr	Ni	Mo	Fe	Mn	Si
Stellite 21	0.28	Bal.	27.0	2.75	5.5	1.0	0.60	0.60
High-carbon Stellite 21	.38	Bal.	27.0	2.75	5.5	1.0	.50	.50

TABLE II - AVERAGE CENTRIFUGAL STRESS AT 11,500 rpm IN TURBINE BLADES

AT POINT OF MAXIMUM TEMPERATURE<sup>a</sup>

Type of Stellite 21	Stress (psi)
Production	20,700
High carbon	21,000
Fine grain	20,600
Medium grain	20,400
Coarse grain	20,100

<sup>a</sup>Two inches above base of blade.

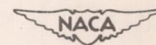
TABLE III - RESULTS OF ENGINE OPERATION OF TURBINE BLADES

Type of Stellite 21	Failure Time		
	Order of failure	Hours at rated speed (11,500 rpm)	Number of 20-minute cycles
Production	1	41.8	167.40
	2	49.3	197.35
	3	52.2	208.95
	4	82.3	329.50
High carbon	1	68.4	273.75
	2 <sup>a</sup>	69.8	279.30
	3	75.6	302.65
	4	91.1	364.60
	5 <sup>b</sup>	108.9	435.70
Fine grain	1	24.9	99.65
	2	30.3	121.45
	3	31.0	124.30
	4	32.6	130.50
Medium grain	1	29.4	117.55
	2	33.0	132.35
	3	33.6	134.65
	4	34.8	139.35
	5	35.1	140.60
	6	35.1	140.60
	7	36.4	145.60
	8	41.3	165.35
	9	43.9	175.80
Coarse grain	1	27.5	110.35
	2	34.7	138.95
	3	34.8	139.35
	4	35.1	140.60
	5	35.1	140.60

<sup>a</sup>Caused by damage.

<sup>b</sup>One blade still in operating condition after 127 hours at rated speed.

TABLE IV - TOTAL BLADE ELONGATIONS IN ZONES OF MAXIMUM  
ELONGATION PRIOR TO FAILURE

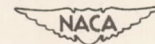


Type of Stellite 21	Failure time (hr)	Elongation (percent in 1/2 inch)	
		Section 3 <sup>a</sup>	Section 4 <sup>b</sup>
Production	41.8	1.66	2.1
	52.2	3.17	2.8
	82.3	3.00	3.3
High carbon	75.6	3.32	4.9
	91.1	5.60	2.8
Fine grain	30.3	1.83	1.8
	31.0	1.70	1.8
	32.6	1.80	2.0
Medium grain	33.0	0.70	1.2
	35.1	.67	1.0
	36.4	.87	1.2
Coarse grain	27.5	0.60	0.5
	34.8	.68	.8
	35.1	.98	.8

<sup>a</sup>  $\frac{3}{8}$  to  $\frac{7}{8}$  inches from blade base.

<sup>b</sup>  $\frac{7}{8}$  to  $2\frac{3}{8}$  inches from blade base.

TABLE V - RESULTS OF GRAIN-SIZE MEASUREMENTS

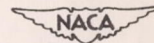


Type of Stellite 21	Failure time (hr)	Grain size		
		<sup>a</sup> Grains per cross section	A.S.T.M. number	
			Range	Av.
Production	41.8	28	---	---
	49.3	29	---	---
	52.2	32	---	---
	82.3	30	---	---
High carbon	68.4	29	---	---
	75.6	15	---	---
	91.1	23	---	---
	108.9	20	---	---
Fine grain	24.9	--	0-4	2
	30.3	--	1-5	2
	31.0	--	2-5	3
	32.6	--	3-6	4
Medium grain	29.4	51	---	---
	33.0	45	---	---
	33.6	42	---	---
	34.8	43	---	---
	35.1	41	---	---
	35.1	27	---	---
	36.4	32	---	---
	41.3	40	---	---
43.9	29	---	---	
Coarse grain	27.5	14	---	---
	34.7	16	---	---
	34.8	10	---	---
	35.1	14	---	---
	35.1	18	---	---

<sup>a</sup>Cross section immediately below failure.

TABLE VI - CHANGE IN HARDNESS DURING ENGINE OPERATION

Type of Stellite 21	Average hardness at failure zone, $R_a$		
	Before operation	After operation	Change
Production	65.5	72.7	7.2
High carbon	66.8	73.8	7.0
Fine grain	69.7	72.4	2.7
Medium grain	69.5	73.2	3.7
Coarse grain	69.8	72.6	2.8



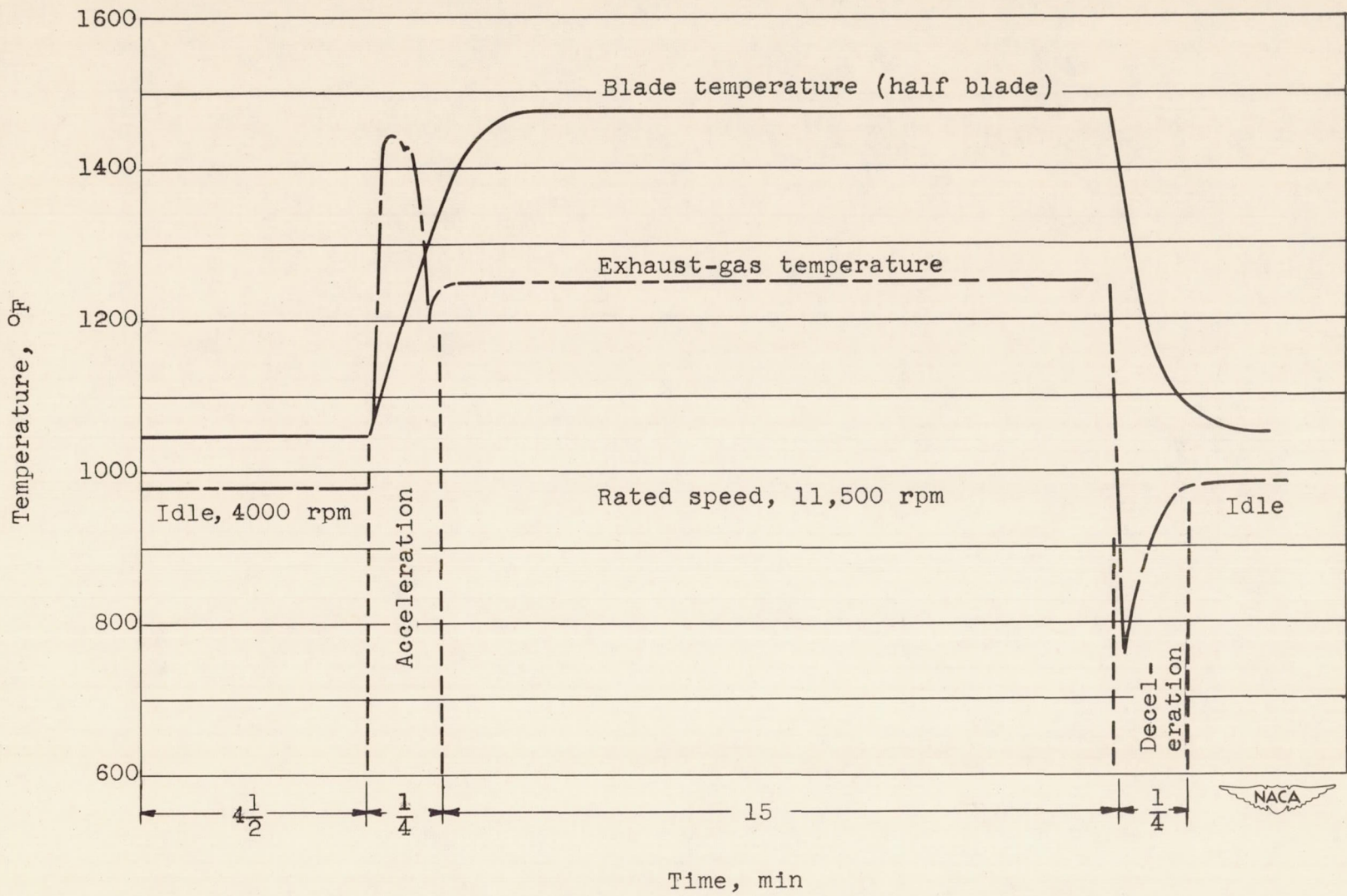


Figure 1. - Temperature conditions during typical engine cycle.

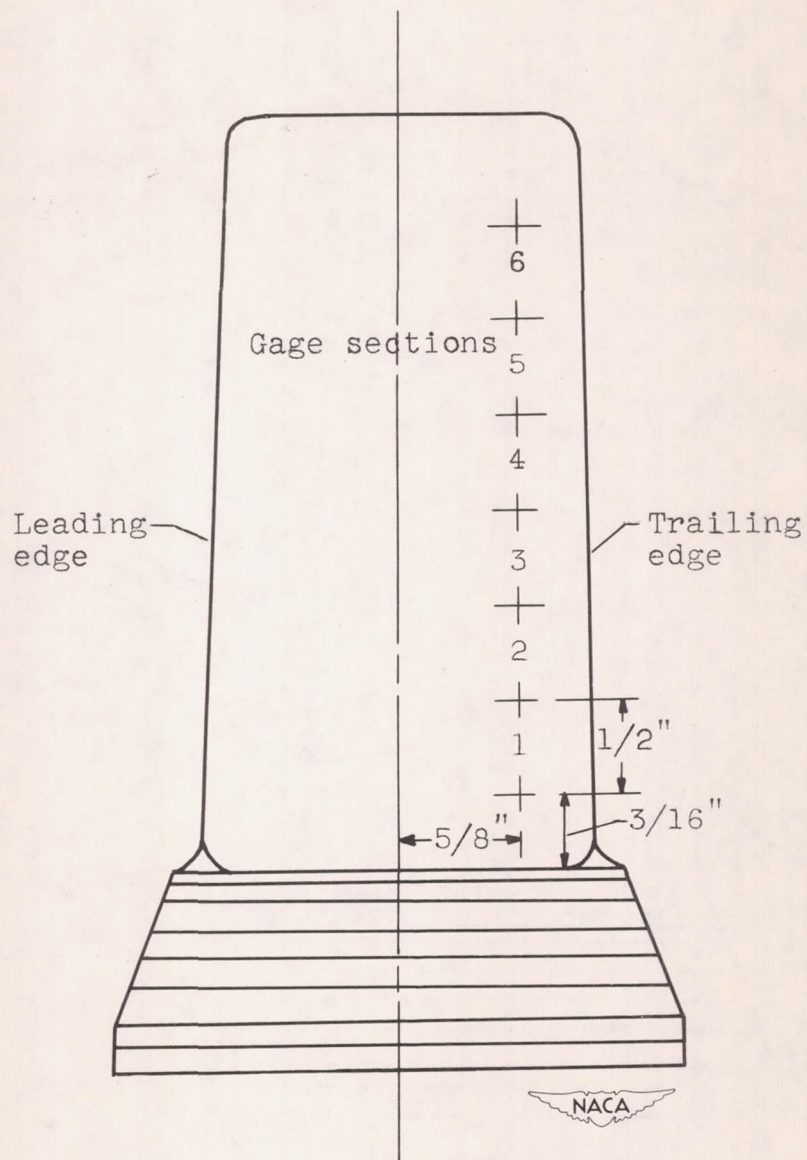


Figure 2. - Location of scribe marks on convex side of turbine blade for use in measuring elongation.

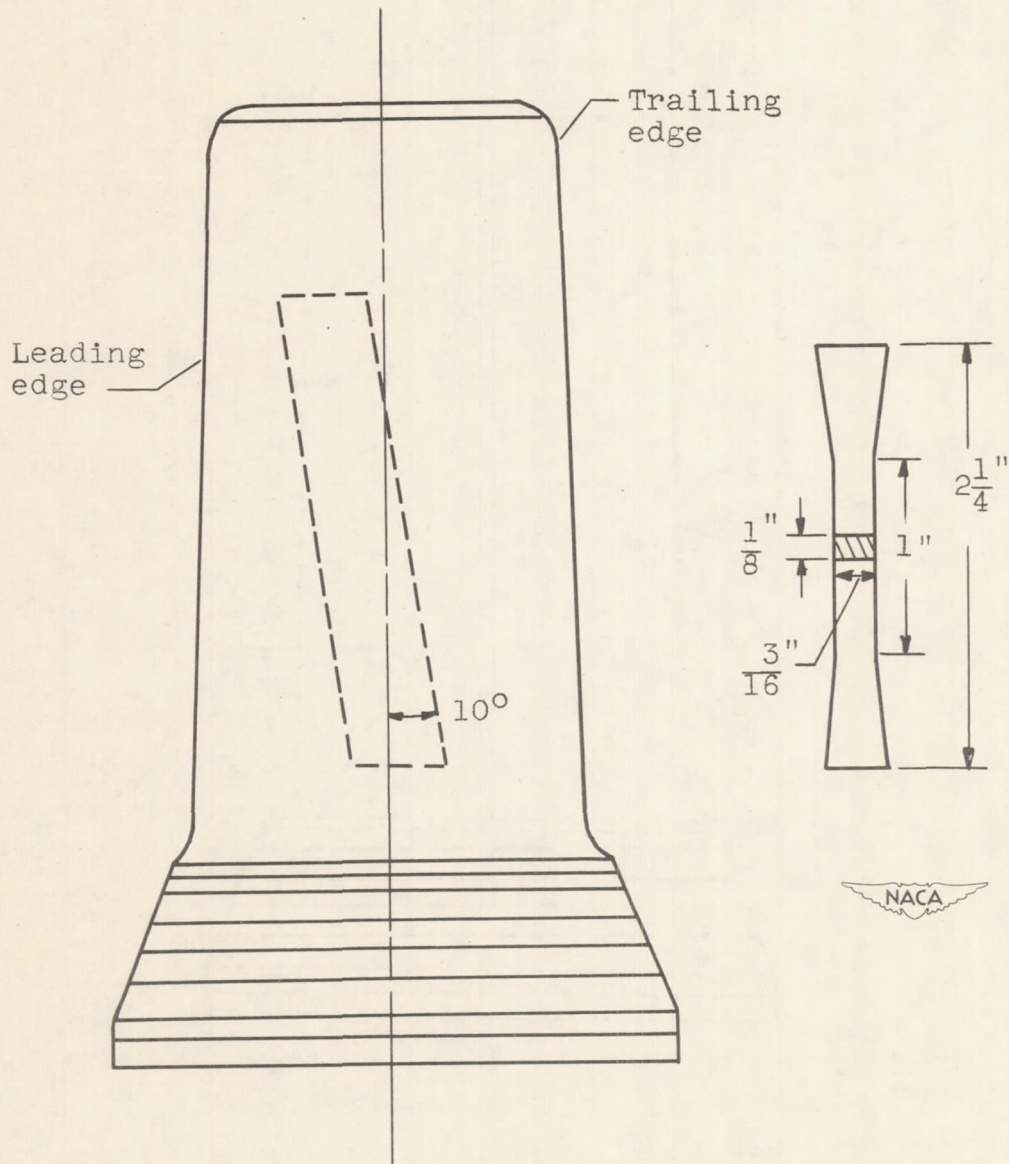


Figure 3. - Blade stress-rupture specimen and zone from which it was machined.

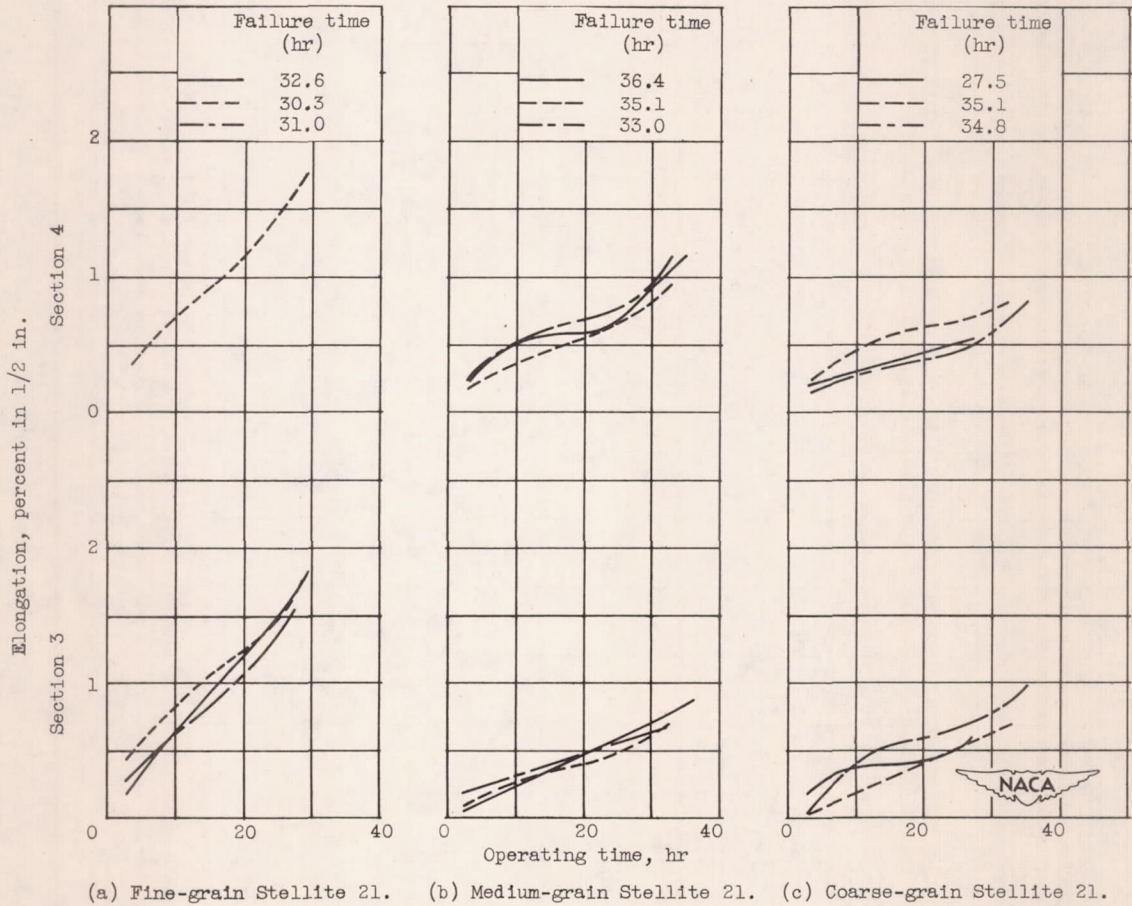


Figure 4. - Creep curves of blades during engine operation.

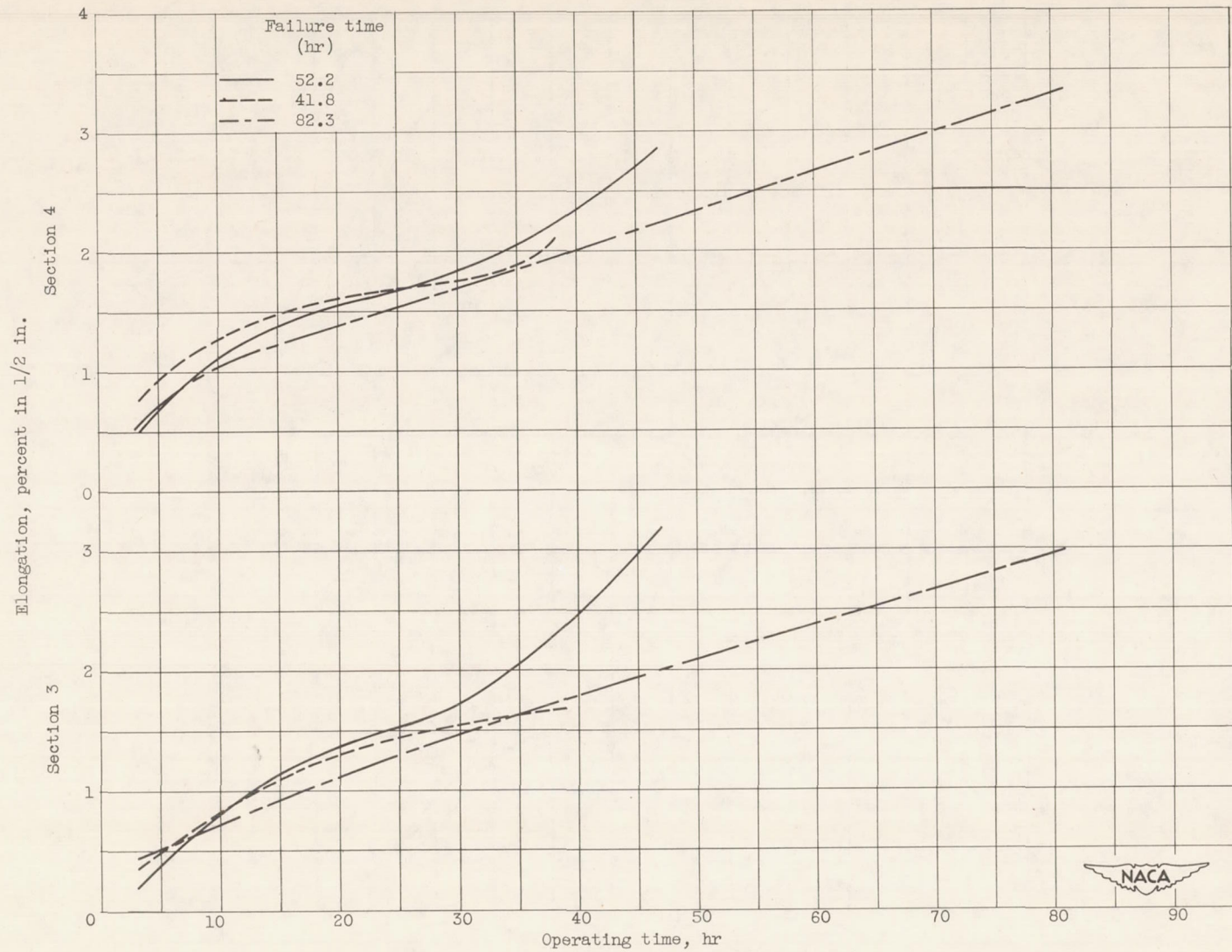
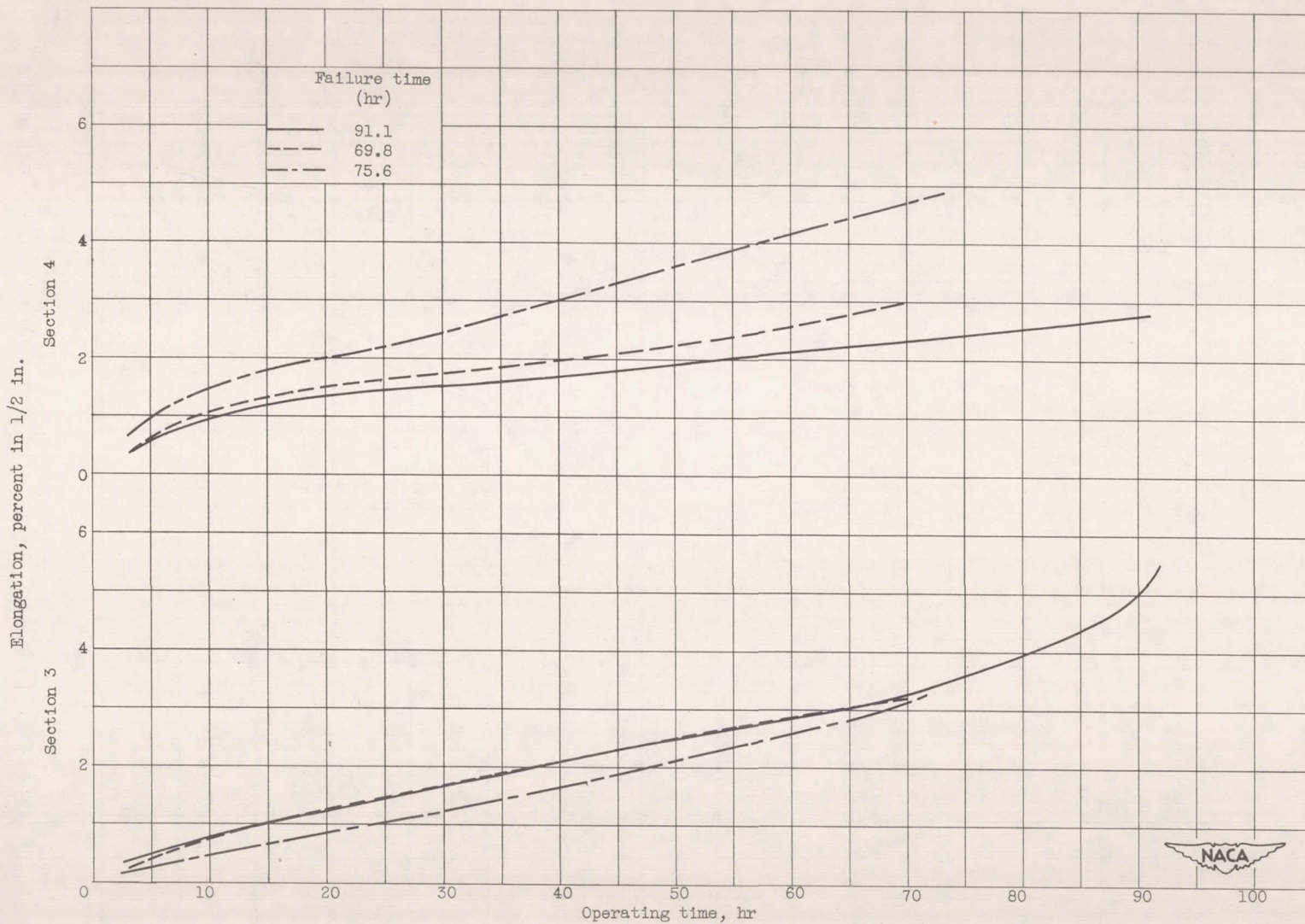


Figure 4. - Continued. Creep curves of blades during engine operation.



(e) High-carbon Stellite 21.

Figure 4. - Concluded. Creep curves of blades during engine operation.

Average elongation in failure zones (3 and 4), percent in 1 in.

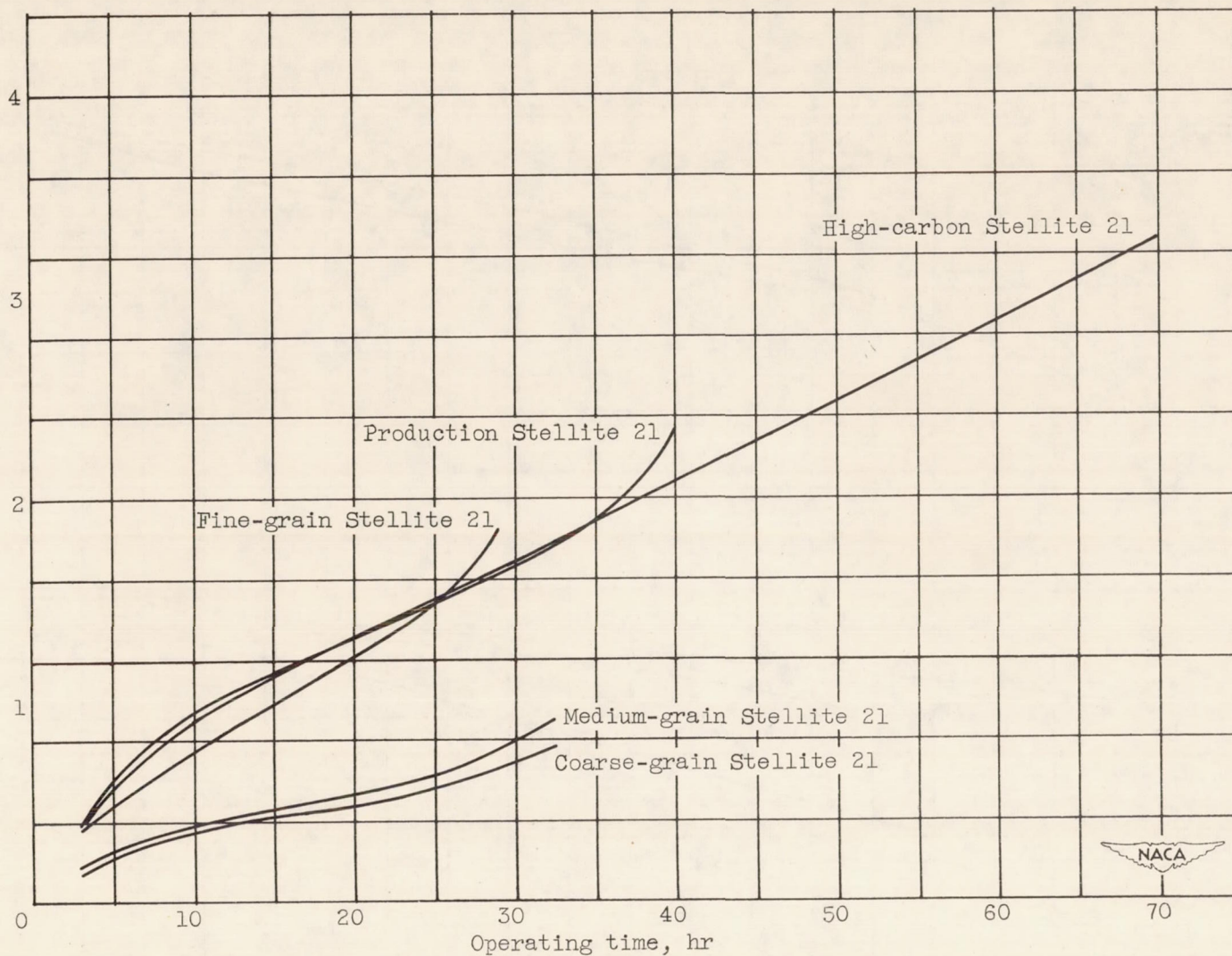
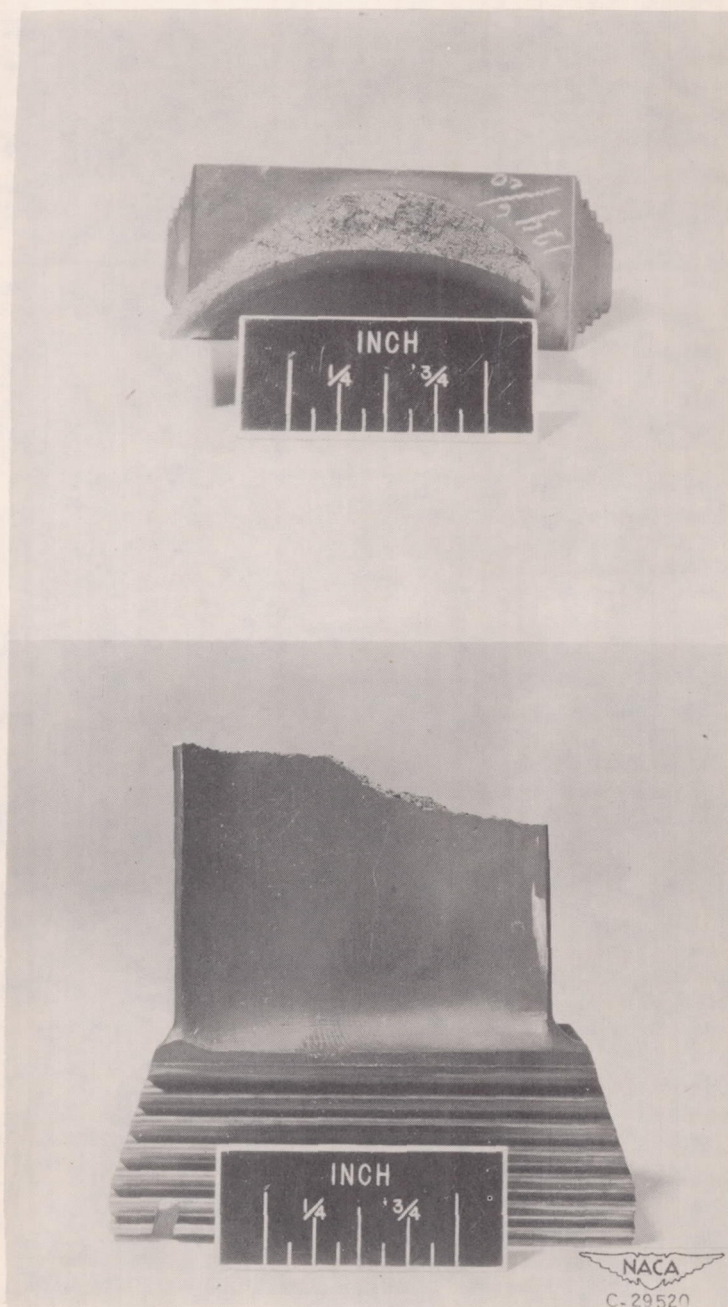
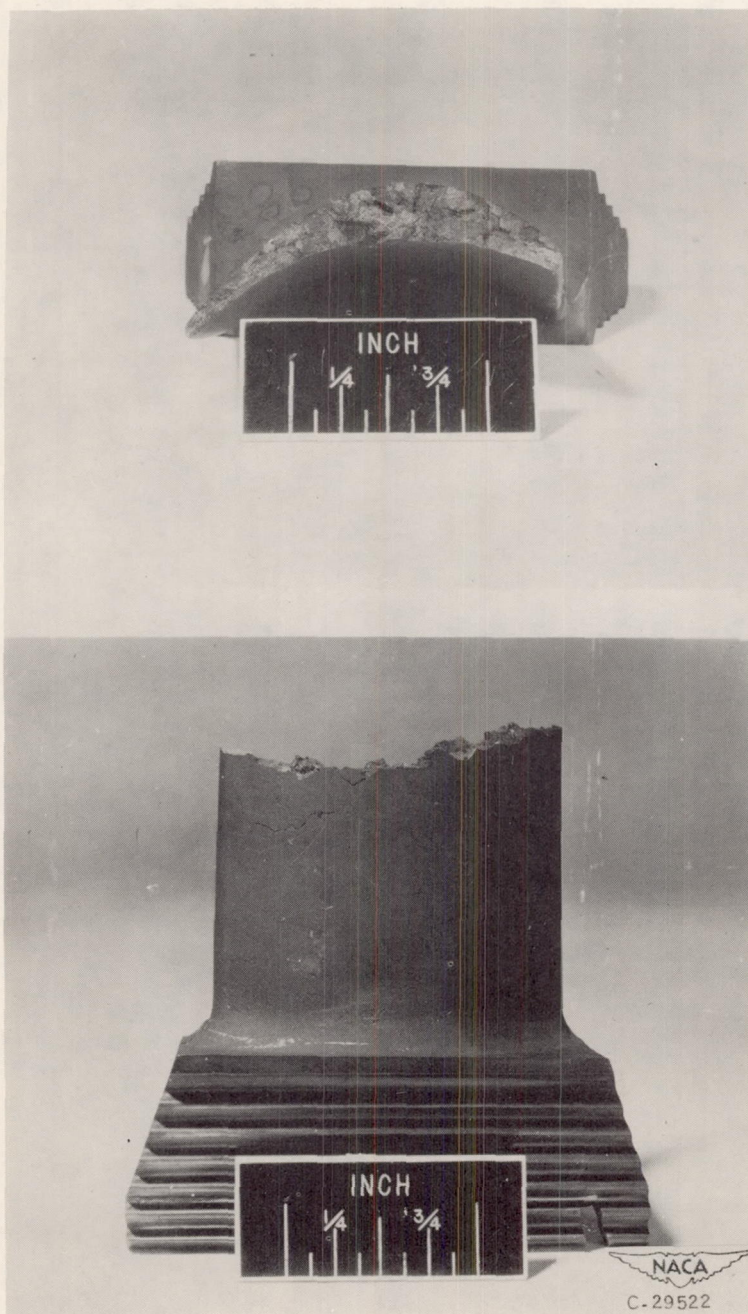


Figure 5. - Comparison of average blade creep.



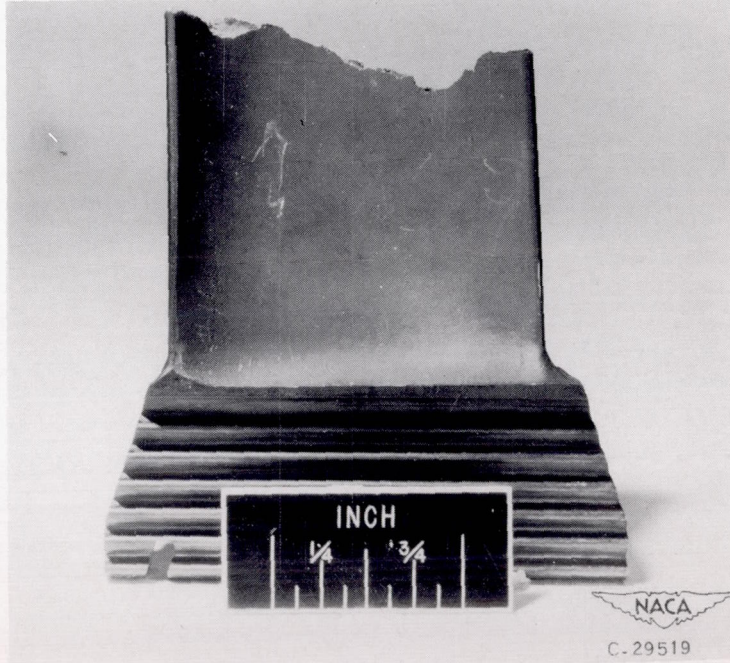
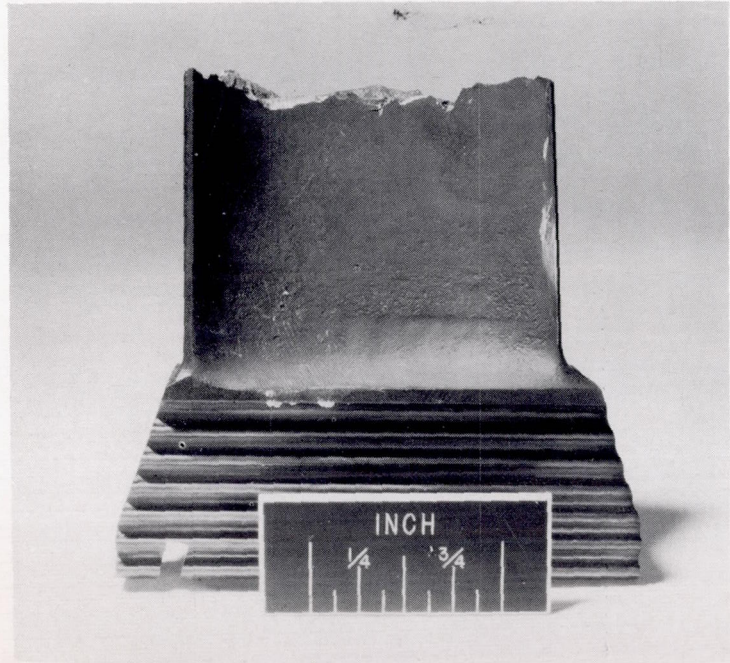
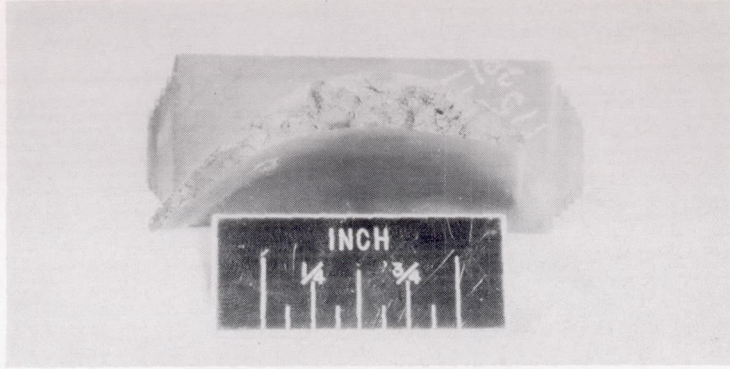
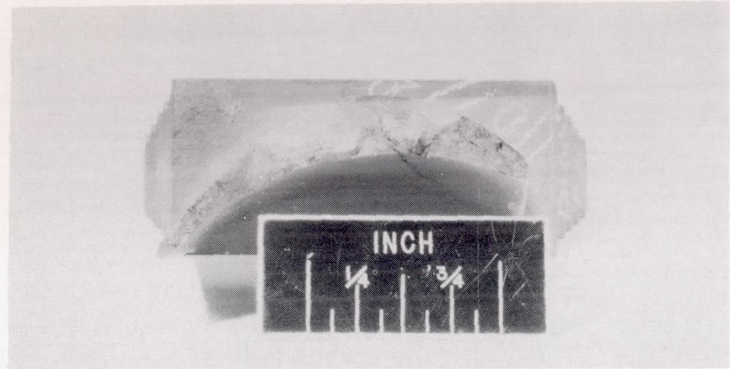
(a) Typical fine grain.

Figure 6. - Blade failures.



(b) Typical medium grain.

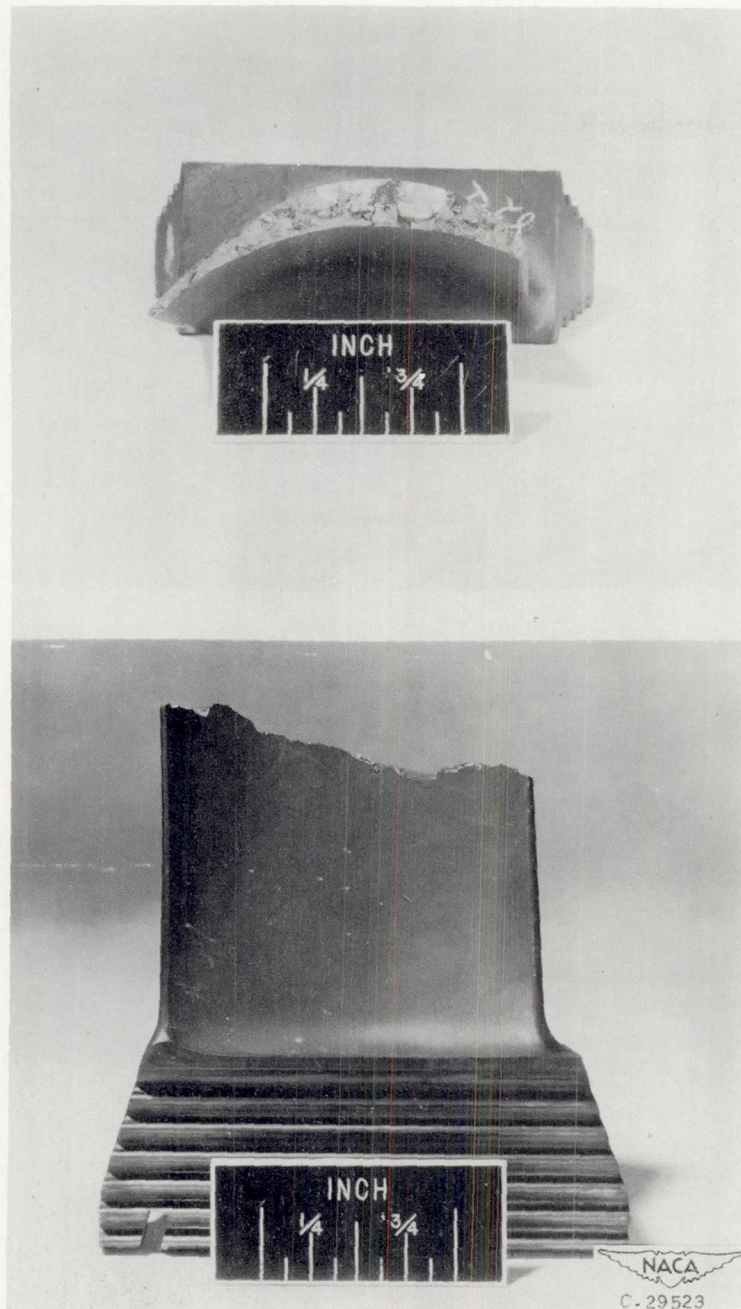
Figure 6. - Continued. Blade failures.



(c) Initial failure coarse grain.

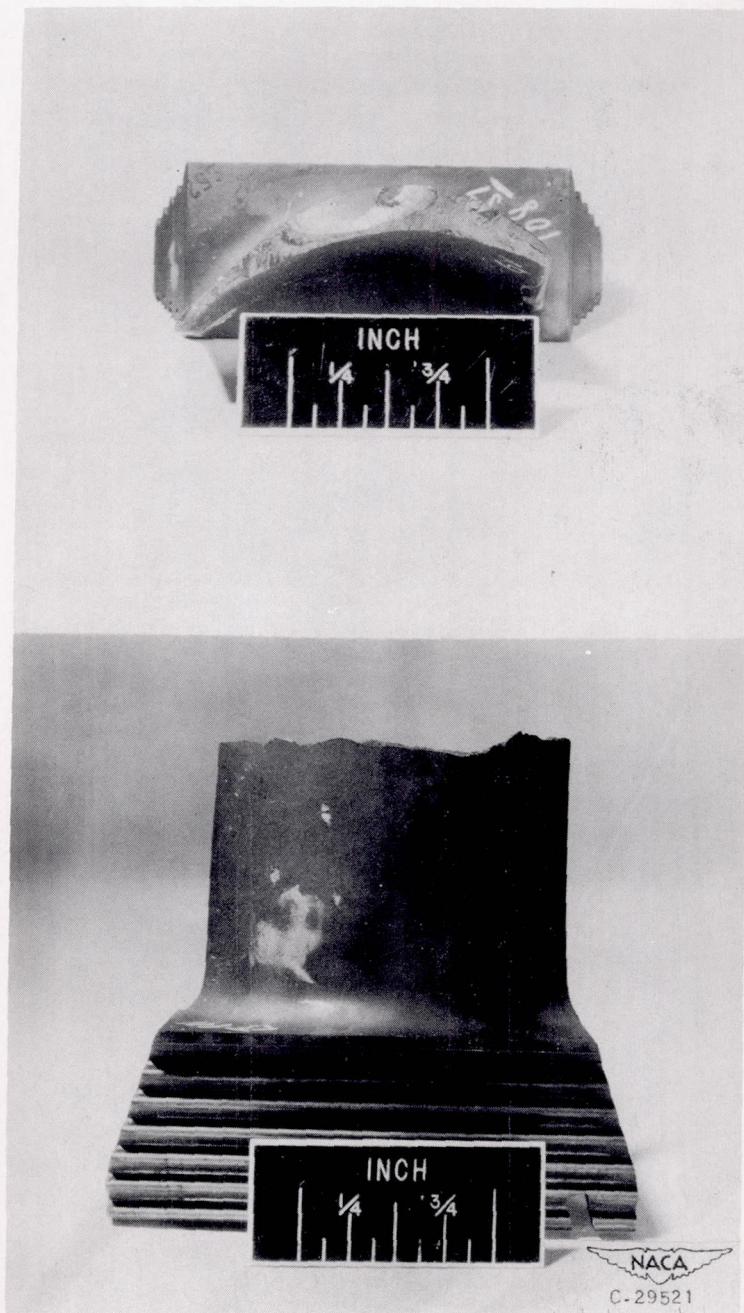
(d) Typical failure coarse grain.

Figure 6. - Continued. Blade failures.



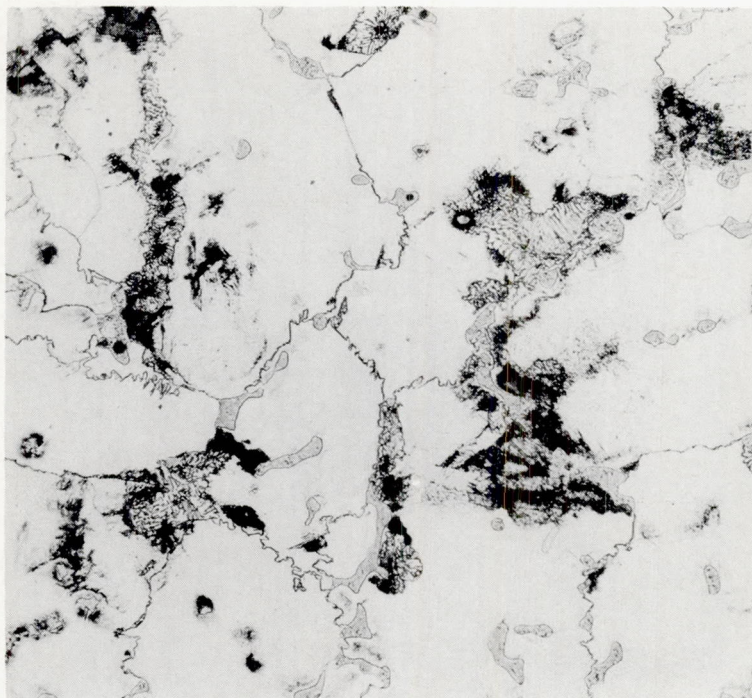
(e) Typical failure of production Stellite 21.

Figure 6. - Continued. Blade failures.

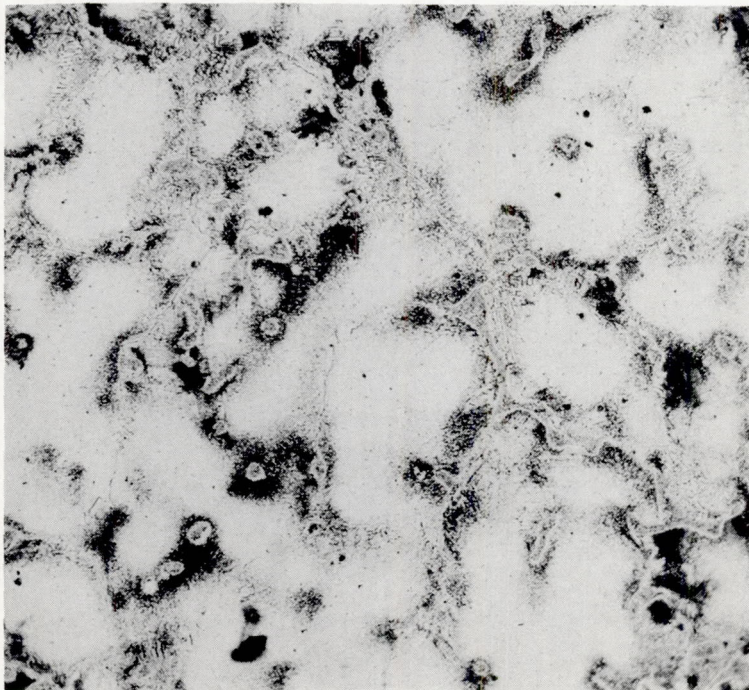


(f) Typical failure of high-carbon Stellite 21.

Figure 6. - Concluded. Blade failures.

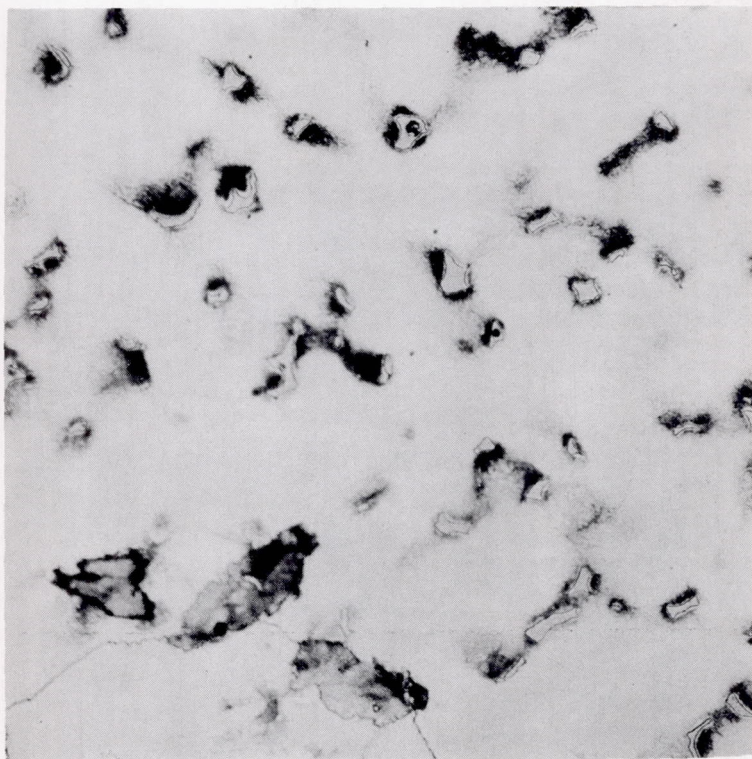


(a) Structure of fine-grain Stellite 21 before operation. Electrolytically etched in 5-percent aqua regia; X250.



(b) Structure of fine-grain Stellite 21 after operation. Electrolytically etched in 5-percent aqua regia; X250.

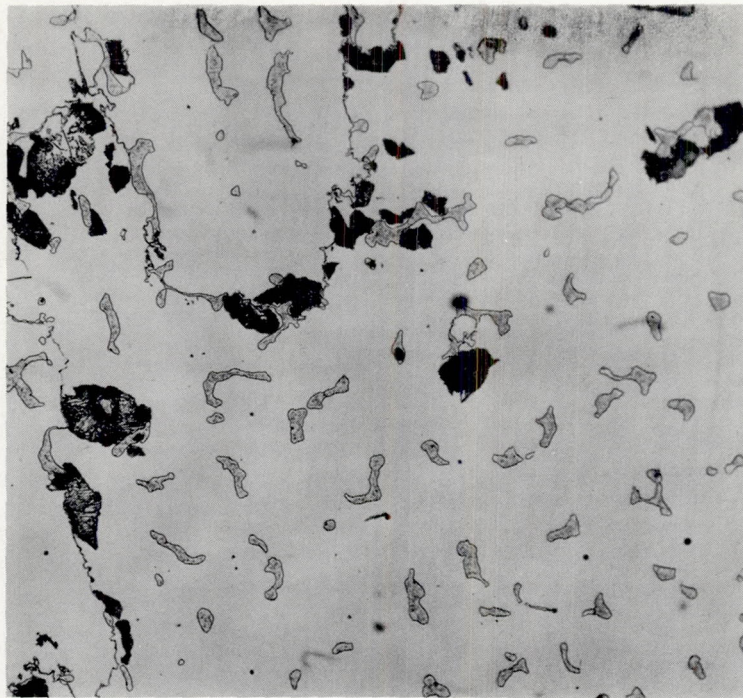
Figure 7. - Typical microstructures.



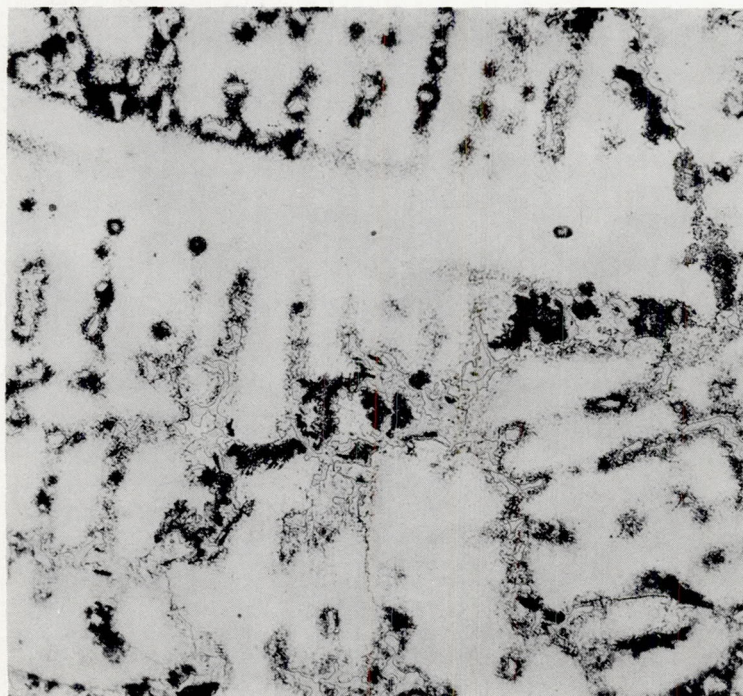
NACA  
C.29512

(c) Structure of medium-grain Stellite 21 before operation. Typical also of coarse-grain Stellite 21 before operation. Electrolytically etched in 5-percent aqua regia; X250.

Figure 7. - Continued. Typical microstructures.

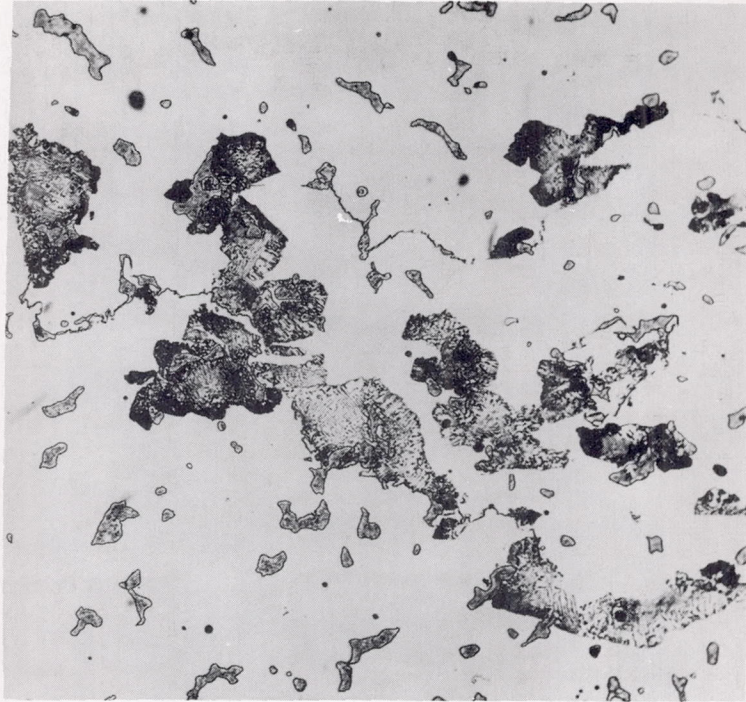


(d) Structure of production Stellite 21 before operation. Electrolytically etched in 5-percent aqua regia; X250.

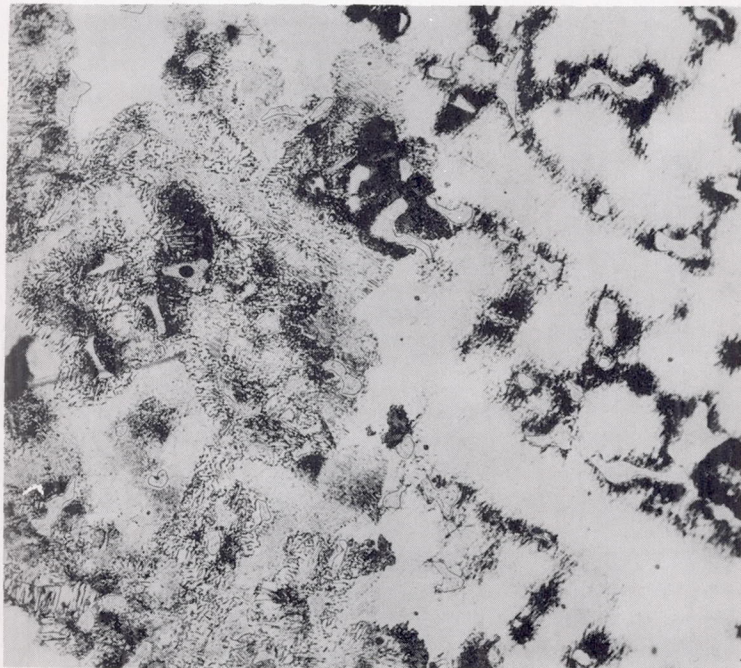


(e) Structure of production Stellite 21 after operation typical of coarse and medium grain size also. Electrolytically etched in 5-percent aqua regia; X250.

Figure 7. - Continued. Typical microstructures.



(f) Structure of high-carbon Stellite 21 before operation. Electrolytically etched in 5-percent aqua regia; X250.

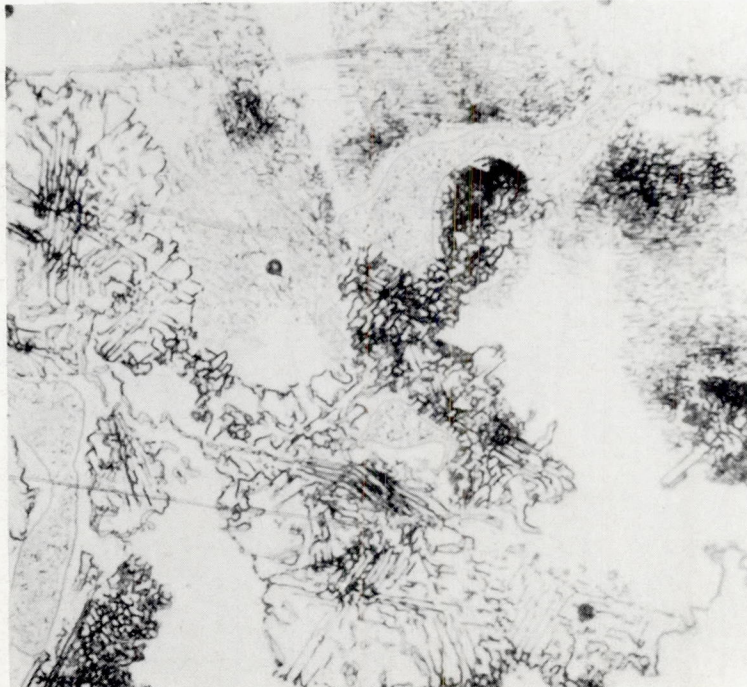


(g) Structure of high-carbon Stellite 21 after operation. Electrolytically etched in 5-percent aqua regia; X250. Note: Dense precipitation in grain boundary zone.

Figure 7. - Continued. Typical microstructures.

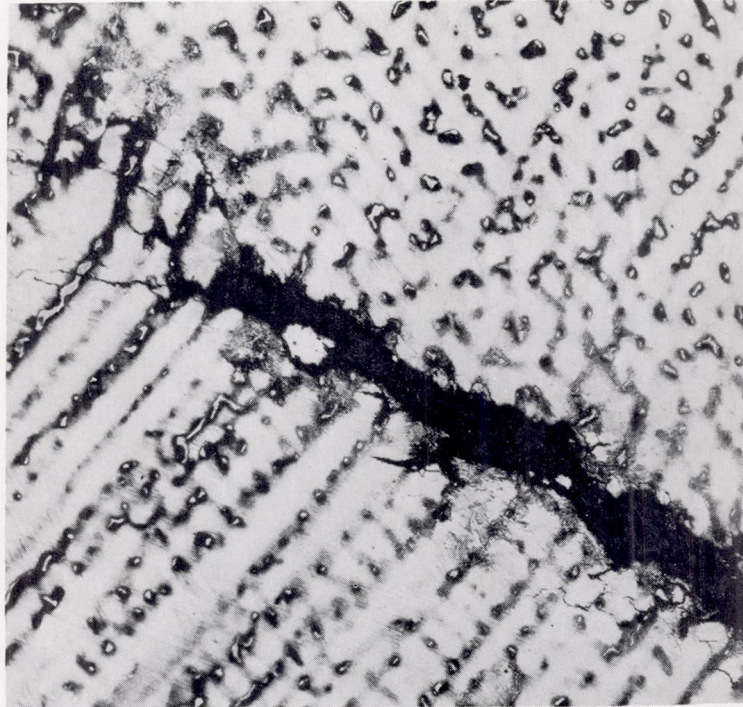


(h) Precipitates in grain boundary zone of high-carbon Stellite 21 blades before operation. Electrolytically etched in 5-percent aqua regia; X1000.

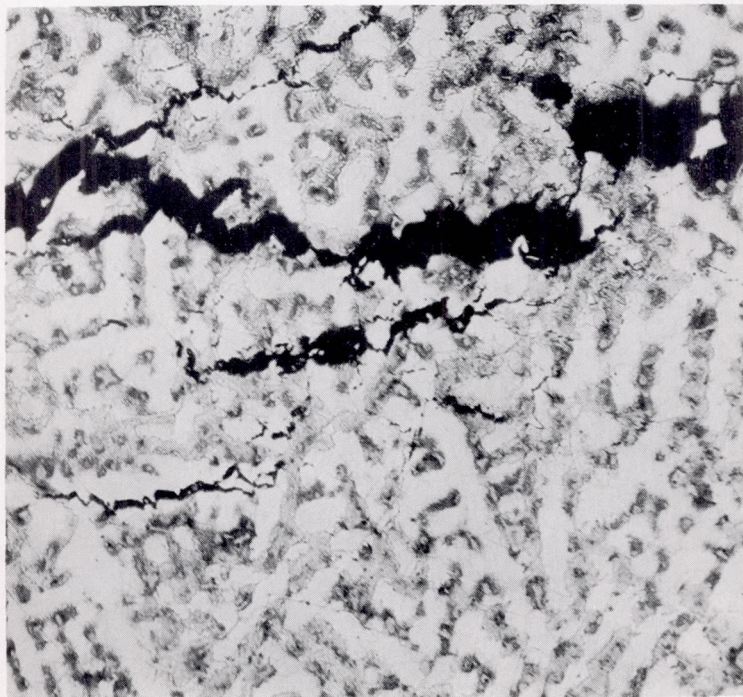


(i) Grain boundary zone of high-carbon Stellite 21 showing precipitates after operation. Electrolytically etched in 5-percent aqua regia; X1000.

Figure 7. - Concluded. Typical microstructures.

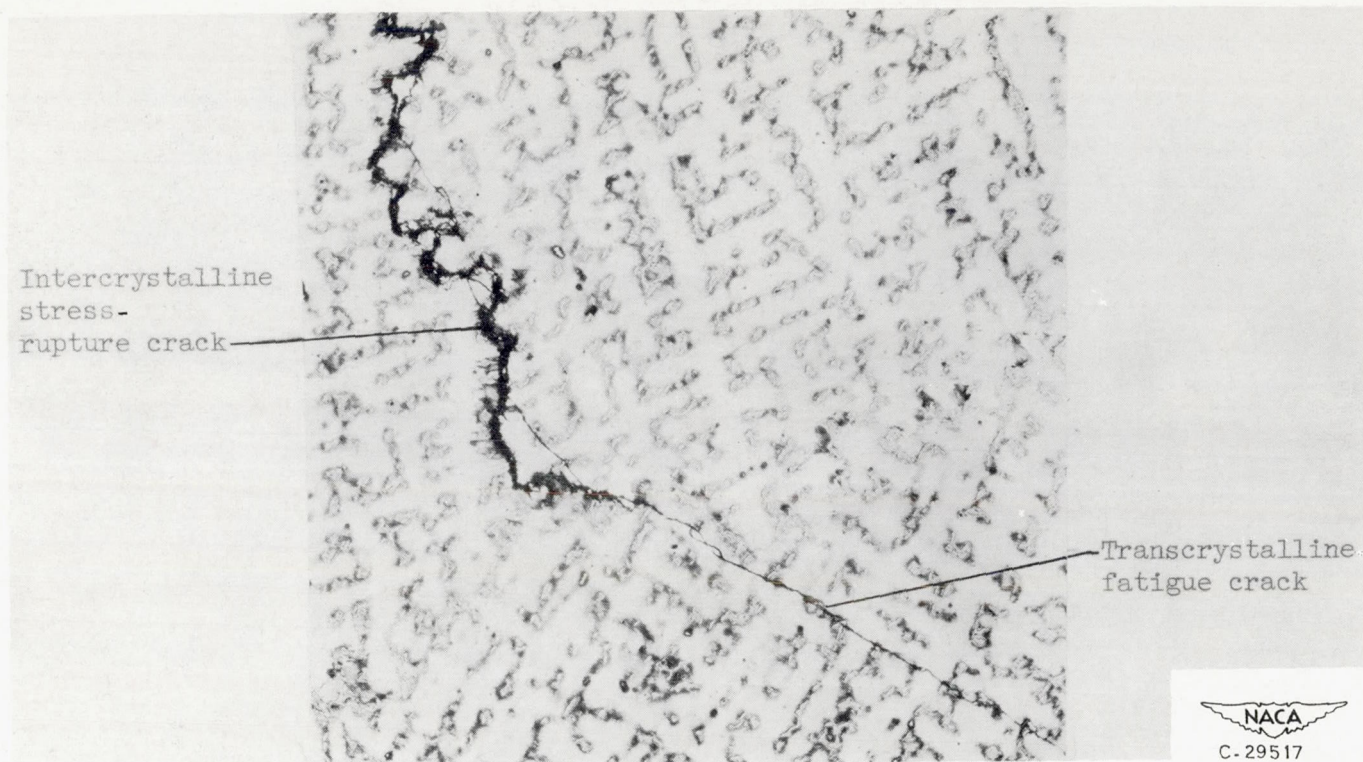


(a) Intercrystalline crack typical of medium- and coarse-grain Stellite 21.



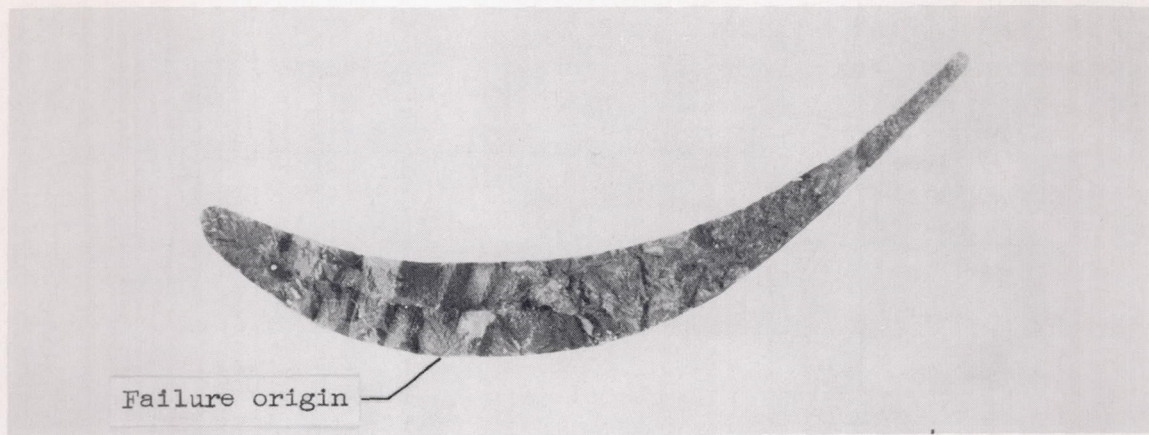
(b) Typical Intercrystalline cracking in fine-grain Stellite 21.

Figure 8. - Typical blade cracks showing fracture paths. All specimens electrolytically etched in 5-percent aqua regia; X100.

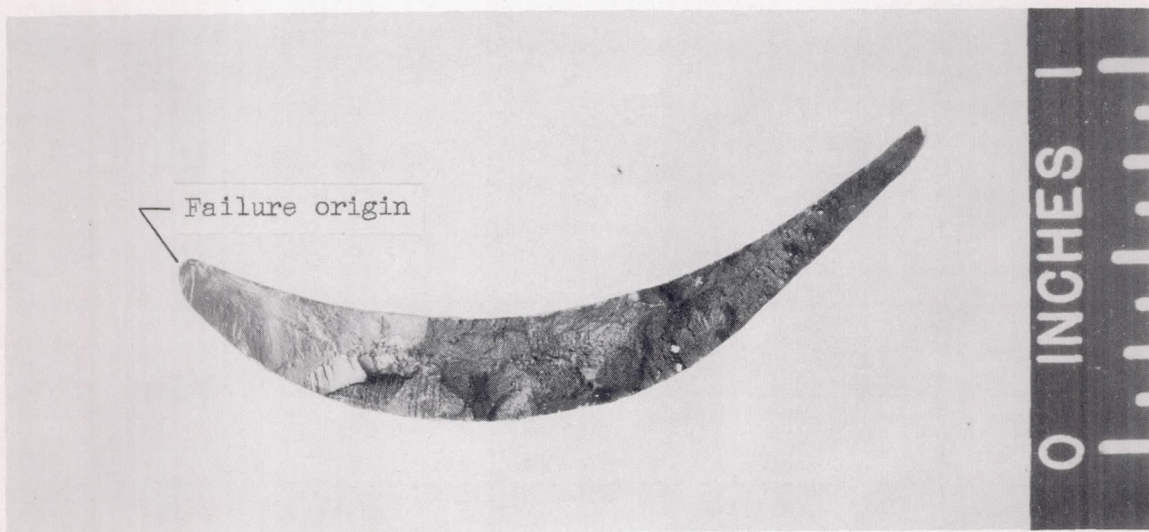


(c) Intercrystalline stress-rupture crack nucleating transcrystalline fatigue crack as is typical in production and high-carbon Stellite 21.

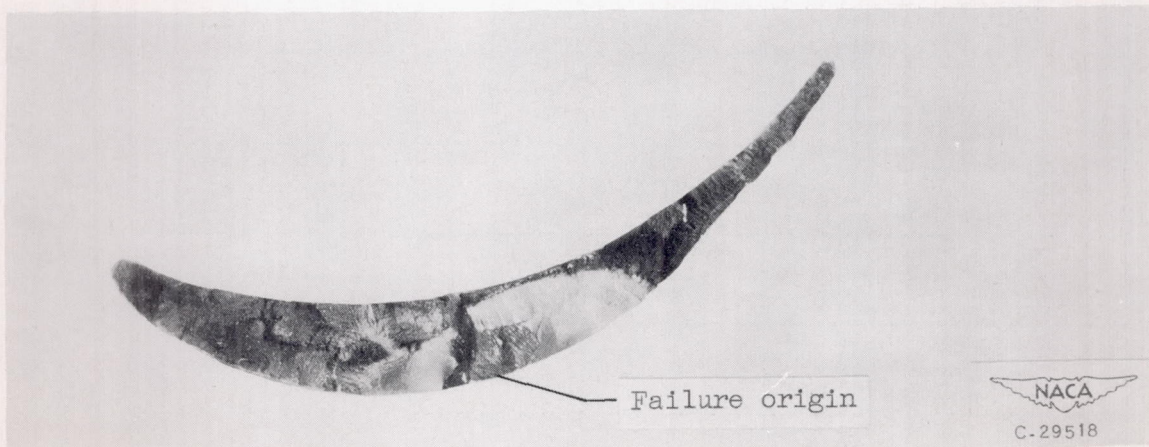
Figure 8. - Concluded. Typical blade cracks showing fracture paths. All specimens electrolytically etched in 5-percent aqua regia; X100.



(a) Stress rupture.



(b) Fatigue.



(c) Stress rupture followed by fatigue.

Figure 9. - Types of blade failure.

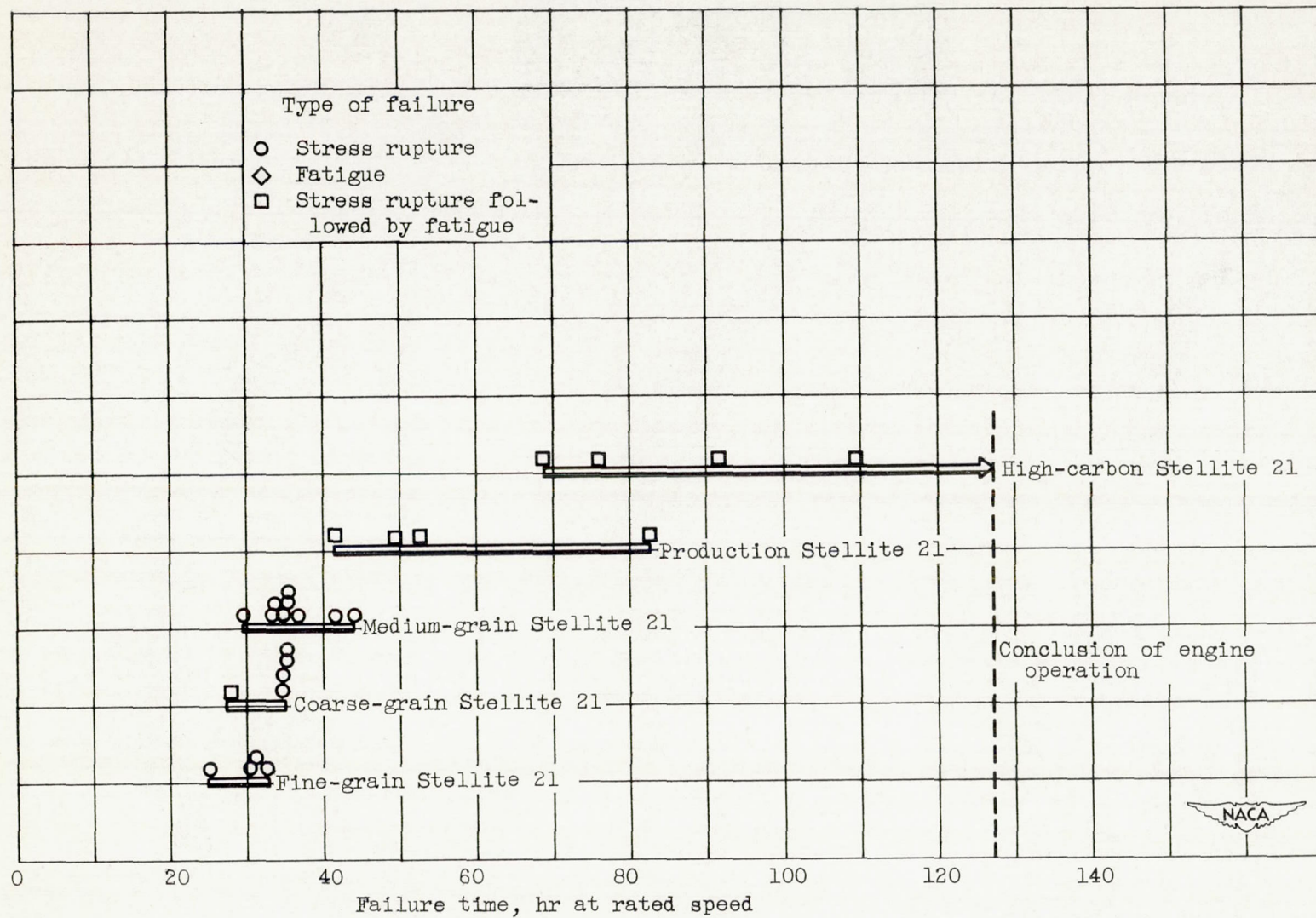


Figure 10. - Results of engine operation.

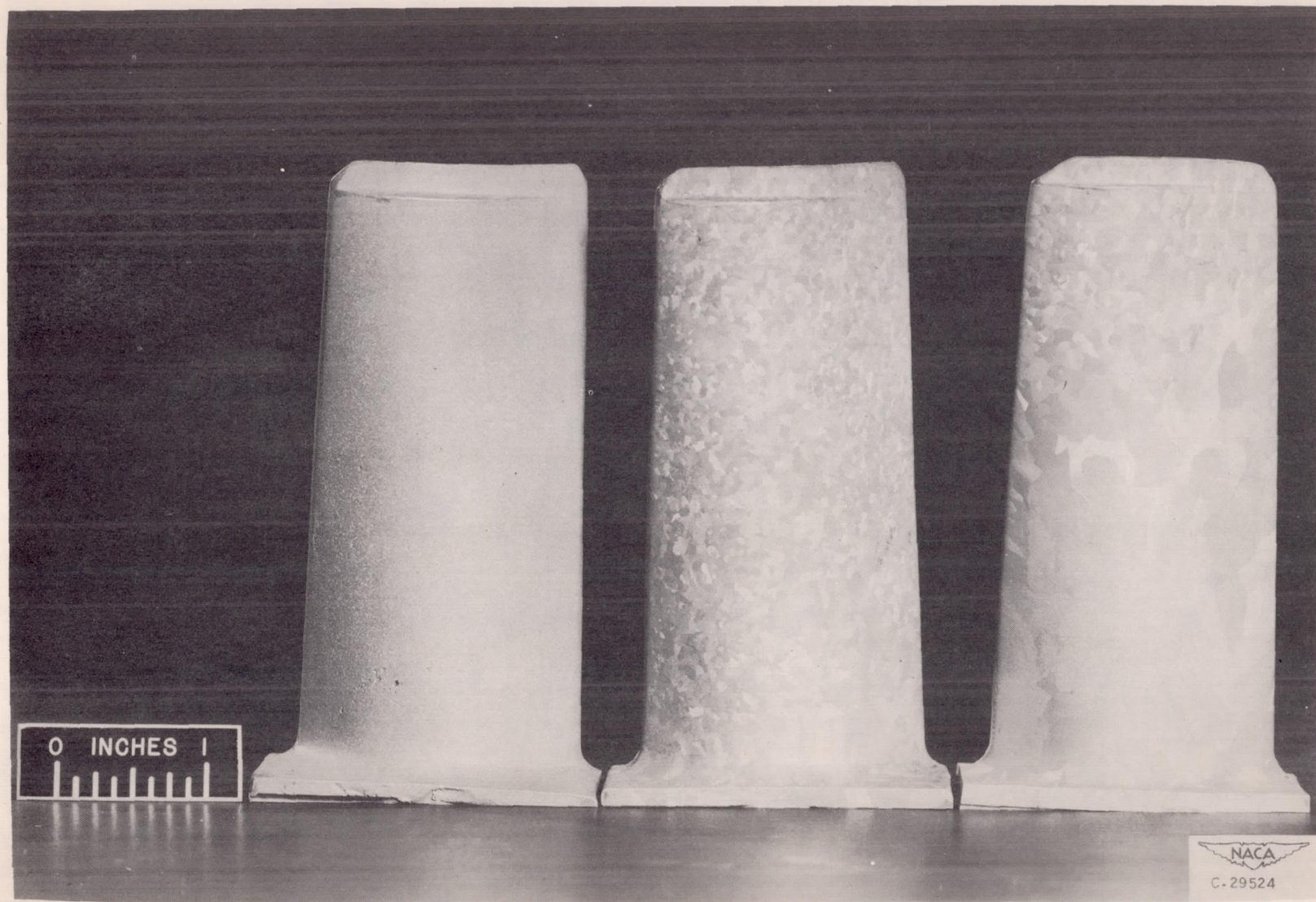


Figure 11. - Controlled grain-size blades macroetched to reveal grain structure.

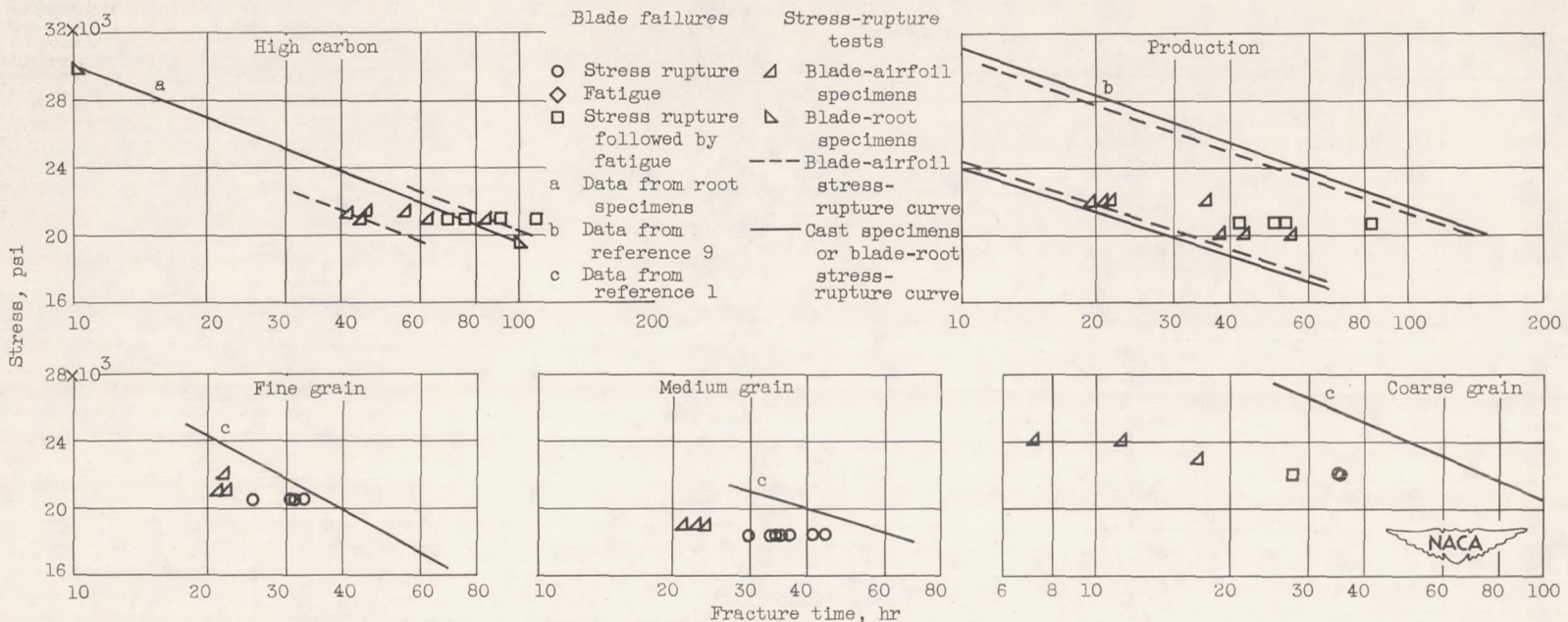


Figure 12. - Comparison of results of stress-rupture and engine evaluations for Stellite 21.